3D PHYSICS-BASED RECONSTUCTION OF SERIALLY ACQUIRED SLICES

Stelios Krinidis, Christophoros Nikou and Ioannis Pitas

Aristotle University of Thessaloniki
Department of Informatics
Artificial Intelligence & Information Analysis Lab
Box 451, 54006 Thessaloniki
Greece

ABSTRACT

This paper presents an accurate, computationally efficient, fast and fully-automated algorithm for the alignment of 2D serially acquired sections forming a 3D volume. The method accounts for the main shortcomings of 3D image alignment: corrupted data (cuts and tears), dissimilarities or discontinuities between slices and missing slices. The approach relies on the determination of inter-slice correspondences. The features used for correspondence, are extracted by a 2D physics-based deformable model parameterizing the object shape. Correspondence affinities and global constrains render the method efficient and reliable. The method was evaluated on real images and the experimental results demonstrated its accuracy, as reconstruction errors were smaller than 1 degree in rotation and smaller than 1 pixel in translation.

1. INTRODUCTION

Three-dimensional reconstruction of medical images (tissue sections, CT and autoradiographic slices) is now an integral part of biomedical research. Reconstruction of such data sets into 3D volumes, via the registrations of 2D sections, has gained an increasing interest and the registration of multiple slices is of utmost importance for the correct 3D visualization and morphometric analysis (e.g. surface and volume representation) of the structures of interest. Several alignment algorithms have been proposed in that framework. A review of general medical image registration methods is presented in [1].

The 3D alignment (reconstruction from 2D images) methods may be classified in the following categories: fiducial marker-based methods, feature-based methods using contours, crest lines or characteristic points extracted from the images [2], and gray level-based registration techniques using the intensities of the whole image [3, 4]. Most of the above mentioned techniques do not simultaneously consider the two major difficulties involved in medical image registration.

At first, consecutive slices may differ significantly due to distortions, discontinuities in anatomical structures, cuts and tears. Thus, from this point of view, a registration method must be robust to missing data or outliers [4].

Also, registering the slices sequentially (the second with respect to the first, the third with respect to the second, etc.) leads to different types of misregistration. If an error occurs in the registration of a slice with respect to the preceding slice, this error will propagate through the entire volume [3].

In this paper, a solution to the above mentioned shortcomings is presented. A method determining correspondences between serially acquired slices is proposed. The features used for correspondence, are extracted by a finite element-based model parameterizing the object shape. Although, finite elements are a powerful tool in computer vision applications, they have not yet been extensively considered for the registration of serially acquired slices.

Our approach was motivated by the technique presented in [5], which consists in determining correspondences between objects for recognition using eigen-decomposition analysis. However, our method determines correspondences between slices exploiting contour information obtained by the free vibrations of a initial circular chain (physics-based modeling) [6, 7]. Modal matching using physics-based models assist our method to be robust to missing data. Furthermore, global affinities between correspondences and their filtering render our method more efficient and reliable, overcoming major alignment problems such as distortions.

The remainder of the paper is organized as follows. The physics-based deformable model used as the feature generator is presented in Section 2. In Section 3, the determination of the correspondences between slices is introduced. Experimental results are presented in Section 4 and conclusions are drawn in Section 5.

2. 2D PHYSICS-BASED DEFORMABLE MODELING

Each slice was separately parameterized by the amplitudes of the vibration modes of a physics-based deformable model [6, 7]. The model consists of 2D points sampled on a circular structure, following a circular chain topology [Figure 1.a]. Each model node

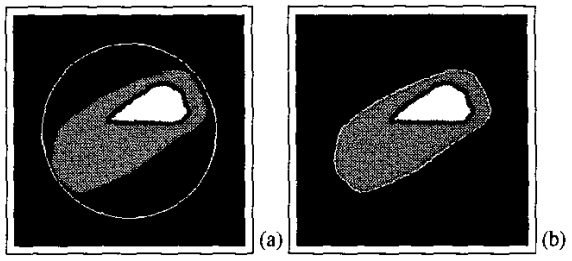

Figure 1: *Parameterization of a 2D slice of a 3D tooth germ volume.* **(a)** *The initial circular chain initialized around the object to be parameterized.* **(b)** *The deformable model at equilibrium (25% of the vibration modes are kept).*

has a mass m and is connected to its two neighbors with springs of stiffness k. The nodes coordinates are stacked in vector

$$\mathbf{X}_0 = (x_1^0, y_1^0, \ldots, x_N^0, y_N^0)^T \quad (1)$$

where N is the number of points of the chain. This physical model is characterized by its mass matrix $\mathbf{M}$, its stiffness matrix $\mathbf{K}$ and

its dumping matrix $\mathbf{C}$, and its governing equation may be written as [8]:

$$\mathbf{M}\ddot{\mathbf{U}} + \mathbf{C}\dot{\mathbf{U}} + \mathbf{K}\mathbf{U} = \mathbf{F} \tag{2}$$

where $\mathbf{U}$ stands for the nodal displacements of the initial circular chain $\mathbf{X}_0$. The image force vector $\mathbf{F}$ is based on the Euclidean distance between the chain nodes and their nearest contour points [9].

Since equation (2) is of order $2N$, where N is the total number of nodes, it is solved in a subspace corresponding to the M truncated vibration modes of the deformable structure [6, 10, 7]. The number of vibration modes retained in the object description, was chosen so as to obtain a compact but adequately accurate representation. A typical *a priori* value for M covering many types of standard deformations is the quarter of the number of degrees of freedom of the system (i.e. 25% of the modes were kept).

To solve equation (2) in the subspace corresponding to the truncated vibration modes, the following change of basis is applied:

$$\mathbf{U} = \mathbf{\Phi}\tilde{\mathbf{U}} = \sum_{i=1}^{M} \tilde{u}_i \phi_i \tag{3}$$

where $\mathbf{\Phi}$ is a matrix and $\tilde{\mathbf{U}}$ is a vector, ϕ_i is the i^{th} column of $\mathbf{\Phi}$, $\tilde{u}_i$ is the i^{th} scalar component of $\tilde{\mathbf{U}}$ and M is the truncated number of degrees of freedom. By choosing $\mathbf{\Phi}$ as the matrix whose columns are the eigenvectors of the eigenproblem:

$$\mathbf{K}\phi_i = \omega_i^2 \mathbf{M}\phi_i \tag{4}$$

and using the standard Rayleigh hypothesis [6], matrices $\mathbf{K}$, $\mathbf{M}$ and $\mathbf{C}$ are simultaneously diagonalized:

$$\begin{cases} \mathbf{\Phi}^T\mathbf{M}\mathbf{\Phi} = \mathbf{I} \\ \mathbf{\Phi}^T\mathbf{K}\mathbf{\Phi} = \mathbf{\Omega}^2 \end{cases} \tag{5}$$

where $\mathbf{\Omega}^2$ is a diagonal matrix whose elements are the eigenvalues ω_i^2 and $\mathbf{I}$ is the identity matrix.

An important advantage of this formulation is that the eigenvectors and the eigenvalues of a chain with circular topology have an explicit expression [6] and they do not have to be computed by slow eigendecomposition techniques (due to the dimensions of matrices $\mathbf{K}$ and $\mathbf{M}$). The eigenvalues are given by:

$$\omega_p^2 = \frac{4k}{m}\sin^2\left(\frac{p\pi}{N}\right) \tag{6}$$

and the eigenvectors are obtained by:

$$\phi_p = \left[\ldots, \cos\frac{2p\pi n}{N}, \ldots\right]^T \tag{7}$$

where $n \in \{1, 2, \ldots, N\}$.

Substituting (3) into (2) and premultiplying by $\mathbf{\Phi}^T$ yields:

$$\ddot{\tilde{\mathbf{U}}} + \tilde{\mathbf{C}}\dot{\tilde{\mathbf{U}}} + \mathbf{\Omega}^2\tilde{\mathbf{U}} = \tilde{\mathbf{F}} \tag{8}$$

where $\tilde{\mathbf{C}} = \mathbf{\Phi}^T\mathbf{C}\mathbf{\Phi}$ and $\tilde{\mathbf{F}} = \mathbf{\Phi}^T\mathbf{F}$.

In many computer vision applications [7], when the initial and the final state are known, it is assumed that a constant load $\mathbf{F}$ is applied to the body. Thus, equation (2) is called the equilibrium governing equation and corresponds to the static problem:

$$\mathbf{K}\mathbf{U} = \mathbf{F} \tag{9}$$

In the new basis, equation (9) is thus simplified to $2N$ scalar equations:

$$\omega_i^2 \tilde{u}_i = \tilde{f}_i \tag{10}$$

In equation (10), ω_i designates the i^{th} eigenvalue and the scalar $\tilde{u}_i$ is the amplitude of the corresponding vibration mode (corresponding to eigenvector ϕ_i). Equation (10), indicates that instead of computing the displacements vector $\mathbf{U}$ from equation (9), we can compute its decomposition in terms of the vibration modes of the original chain.

Figure 1 illustrates the vibration modes based parameterization of the 2D slices of a tooth germ volume. The 25% lowest frequency modes were retained for this representation as this truncated description provides a satisfactory compromise between accuracy and complexity of the representation. The circular chain is initialized around each slice [Fig. 1(a)] and the vibration amplitudes are explicitly computed by equation (10), where rigid body modes ($\omega_i = 0$) are discarded and the nodal displacement may be recovered using equation (3). The physical representation $\mathbf{X}(\tilde{\mathbf{U}})$ is finally given by applying the deformations to the initial circular chain:

$$\mathbf{X}(\tilde{\mathbf{U}}) = \mathbf{X}_0 + \mathbf{\Phi}\tilde{\mathbf{U}} \tag{11}$$

Thus, each slice of the 3D volume is described in terms of vibrations of an initial chain (Fig. 1(b)).

3. MODAL CORRESPONDENCES

Having approached the object contours using the physics-based deformable model (eq. 11) the next step is to determine inter-slice correspondences between the model parameters.

To determine correspondences, we use vector $\mathbf{U}$ (eq. 3), expressed as:

$$\mathbf{U} = \mathbf{\Phi}\tilde{\mathbf{U}} = \left[\mathbf{\Phi}_1\tilde{\mathbf{U}}_1 | \ldots | \mathbf{\Phi}_M\tilde{\mathbf{U}}_M\right] = \left[\ x_1 \cdots x_N y_1 \cdots y_N\ \right]^T \tag{12}$$

where M denotes the number of retained modes and (x_i, y_i) describes the displacement of the i^{th} feature point at X and Y axis respectively.

Thus, in order to determine the correspondences between two slices Q and S, we build vectors $\mathbf{U}^Q$ and $\mathbf{U}^S$ respectively and compare these parameterized displacement vectors. The comparison is based on the following criteria:

3.1. Affinity Matrix

We now compute what are referred to as the affinities between the two sets of parameterized displacement vectors (eq. 12). These are stored in an *affinity matrix* $\mathbf{Z}^{QS}$, where:

$$z_{ij}^{QS} = \left\|x_i^Q - x_j^S\right\|^2 + \left\|y_i^Q - y_j^S\right\|^2 \tag{13}$$

where $\|\cdot\|^2$ denotes the L_2 norm and Q and S are the slices under examination. The affinity measure z_{ij}^{QS} for the i^{th} and j^{th} points (of slices Q and S respectively), is zero for a perfect match and increases as the match worsens. Using that affinity measure, we can easily identify which features correspond to each other in the two slices by looking for a minimum entry in each column and row of $\mathbf{Z}^{QS}$. Because of the reduced basis matching, similarity of the generalized features is required in both directions instead of one direction only. In other words, a match between the i^{th} feature in a certain slice and the j^{th} feature in a candidate slice can only be valid if z_{ij}^{QS} is the minimum value for its row, and z_{ji}^{QS} the minimum for its column.

3.2. Outliers Rejection

A measure d^{QS} expressing the continuity of correspondences (belonging to slices Q and S), is also computed:

$$d^{QS}(p_i^Q) = \left|Order(p_i^Q) - Order(\Theta^S(p_i^Q))\right| \tag{14}$$

where p_i^Q denotes the i^{th} point of slice Q, $\Theta^S(p_i^Q)$ its correspondent point on slice S and $|\cdot|$ the L_1 norm. $Order(\cdot)$ is a function measuring the position of a point with respect to a reference (starting) point. Having computed $d^{QS}(p_i^Q)$ (eq. 14) for all correspondences between slices Q and S, our method accepts only correspondences verifying [11]:

$$d^{QS}(p_i^Q) \leq 1.4826 * \underset{k}{median}\{d^{QS}(p_k^Q)\} \quad (15)$$

3.3. Global Affinities

Let us define a set of functions of type:

$$F^{|Q-S|}(p_i^Q, p_j^S) = \begin{cases} 1, & \text{if point } p_i^Q \text{ corresponds to } p_j^S \\ 0, & \text{if there is no correspondence} \end{cases} \quad (16)$$

where p_i^Q is the i^{th} point of slice Q and p_j^S is the j^{th} point of slice S. Let us also consider the set of correspondences $\boldsymbol{C}_{Q,S}^{|Q-S|}$ between slices Q and S as the the union:

$$\boldsymbol{C}_{Q,S}^{|Q-S|} = \bigcup_i^N \bigcup_j^N F^{|Q-S|}(p_i^Q, p_j^S) \quad (17)$$

where N is the total number of the physics-based deformable model points. Finally, we define the set of correspondences between equidistant slices:

$$\boldsymbol{\mathcal{E}}^n = \boldsymbol{C}_{1,n+1}^n \bigcup \boldsymbol{C}_{2,n+2}^n \bigcup \cdots \bigcup \boldsymbol{C}_{M-n,M}^n \quad (18)$$

where M is the total number of slices and n is the distance between the slices under examination. If n is equal to 1 then point correspondences are restricted to successive slice pairs.

Global affinities exploit and combine information from all point correspondence sets, in successive pairs $\boldsymbol{\mathcal{E}}^1$, triplets $\boldsymbol{\mathcal{E}}^2$, etc. By these means any remaining fault correspondences are discarded.

More practically, assume that we have the correspondence sets $\boldsymbol{\mathcal{E}}^1$ and $\boldsymbol{\mathcal{E}}^2$. A correspondence between point p_i^n of the n^{th} slice and p_j^{n+1} of slice $n+1$ is valid only if:

$$F^1(p_i^n, p_j^{n+1}) * F^1(p_i^n, p_k^{n-1}) * F^2(p_k^{n-1}, p_j^{n+1}) = 1 \quad (19)$$

where k is a point belonging to the (n-1)th slice, and is used for the completion of the chain. If expression (19) is verified the initial correspondence between points p_i^n and p_j^{n+1} is accepted, otherwise it is discarded.

The overall correspondence establishment algorithm is summarized as follows:

- deform the initial circular physics-based model on each slice separately (eq. 9-11).
- compute correspondence affinities (eq. 13).
- eliminate outliers (eq. 14).
- determine the correspondences between successive slices ($\boldsymbol{\mathcal{E}}^1$, $\boldsymbol{\mathcal{E}}^2$, etc), (eq. 18).
- for each correspondence **do**
  - find the necessary points satisfying the global cost function (eq. 16) and calculate expression (19) for these points.
  - **if** (19) is equal to zero, discard the correspondence.
  - **else** accept the correspondence.
- **end do**

The next step is to determine the rigid transformation parameters (2D rotation and translation) aligning the respective slices. The rotation matrix $\mathbf{R}$ and the translation vector $\mathbf{T}$ are estimated for each slice, in order to minimize the mean square error between the remaining corresponding points using the method described in [12].

4. EXPERIMENTAL RESULTS

To evaluate our method, we applied the proposed algorithm to the reconstruction of an artificially misaligned 3D human skull (Figure 2). The slices of the original 256 × 256 × 140 CT volume were transformed using translations varying from -10 to +10 pixels and rotations varying from -40 to +40 degrees. The transformations for each slice were random following a uniform distribution in order not to privilege any slice [Fig. 2(a) and 2(b)]. Human skull volume presents discontinuities, and consecutive slices may differ significantly due to anatomy but the correspondence evaluation was proved robust to these shortcomings. Table 1 presents statistics on the alignment errors. As it can be seen, median and mean translation and rotation errors are less than 1 pixel and 1 degree

Alignment error statistics

	Δt_x	Δt_y	$\Delta\theta$
median	0.19	0.23	0.13
maximum	1.18	1.07	1.42
mean ± s. dev	0.29 ± 0.26	0.31 ± 0.26	0.33 ± 0.34

Table 1: *A set of 140 slices of a 3D CT human skull volume were artificially transformed using different rigid transformation parameters. Each slice was randomly transformed using translations varying from -10 to +10 pixels and rotations varying from -40 to +40 degrees. Different statistics on the errors for the rigid transformation parameters are presented. Translation errors are expressed in pixels and rotation errors in degrees.*

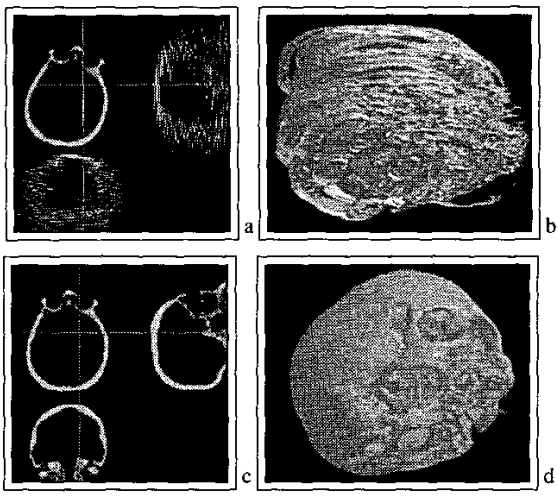

Figure 2: *Reconstruction of a 3D human skull volume of 140 slices.* **(a)** *Multiplanar view of the volume before registration.* **(b)** *Three-dimensional view of the volume before registration.* **(c)** *Multiplanar view of the volume after registration.* **(d)** *Three-dimensional view of the volume after registration.*

respectively. Also maximum errors are slightly larger than 1 pixel and 1 degree respectively, showing the robustness of the proposed technique. Fig. 2(c) and 2(d) present the reconstructed volume.

Furthermore, the algorithm was applied to the reconstruction of volumes (tooth germs) with unknown ground truth. The performance of our method was compared with the manual alignment accomplished by an expert physician-researcher. Figure 3 shows the reconstruction of a tooth germ by an expert dentist-researcher [Fig. 3(a) and 3(b)] and by our method [Fig. 3(c) and 3(d)]. It is illustrated that human intervention fails to correctly align the slices, whilst our method is efficient and can achieve alignment with higher accuracy, as confirmed by dentist specialists-researchers. In the example, the smoothness and the low curvature of the teeth surface aligned by our algorithm is of better visual quality.

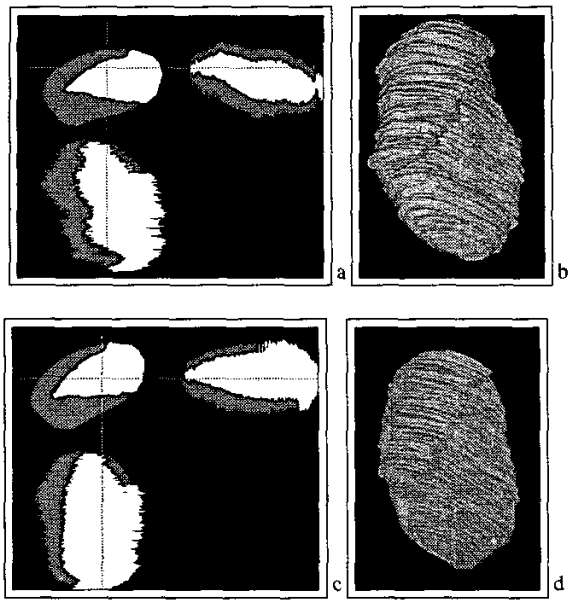

Figure 3: *Reconstruction of a 3D tooth germ volume of 265 slices.* **(a)** *Multiplanar and* **(b)** *3D view of the volume after manual alignment by an expert dentist.* **(c)** *Multiplanar and* **(d)** *3D view of the volume after registration.*

Finally, let us notice that the algorithm has a computational complexity $O(NM)$, where N is the number of slices and M is the number of nodes of the deformable model. It requires approximately 1 min. to reconstruct a 256 × 256 × 140 volume on a Pentium III (700 MHz) workstation under Windows 2000 Professional without any particular code optimization.

5. CONCLUSIONS

A fast and robust algorithm for the alignment of 2D serially acquired slices was presented. The contours of the slices to be registered were parameterized by a physics-based deformable model and the model parameters were forwarded to several alignment criteria. Local and global constrains were applied to make the technique efficient. At first, alignment was obtained by the computation of an affinity matrix associated with a correspondence continuity measure. The obtained results were fine-tuned by a global affinity metric.

Furthermore, no particular registration direction is privileged by the proposed approach and the use of a global affinity measure eliminates error propagation. Also, the low frequency modal parameterization of the object contours makes the technique robust to missing data or outliers.

The low computation time and the good quality of the alignment with respect to manual techniques makes the method a promising tool for the reconstruction of 3D anatomical structures.

6. REFERENCES

[1] J. B. A. Maintz and M. A. Viergever, "A survey of medical image registration techniques.," *Medical Image Analysis*, vol. 2, no. 1, pp. 1–36, 1998.

[2] A. Rangarajan, H. Chui, E. Mjolsness, S. Pappu, L. Davachi, P. Goldman-Rakic, and J. Duncan, "A robust point-matching algorithm for autoradiograph alignment.," *Medical Image Analysis*, vol. 1, no. 4, pp. 379–398, 1997.

[3] A. Andreasen, A. M. Drewes, J.E. Assentoft, and N. E. Larsen, "Computer-assisted alignment of standard serial sections without use of artificial landmarks. A practical approach to the utilization of incomplete information of 3D reconstruction of the hippocampal region.," *Journal of Neuroscience Methods*, vol. 45, pp. 199–207, 1992.

[4] S. Ourselin, A. Roche, G. Subsol, X. Pennec, and C. Sattonnet, "Automatic alignment of histological sections for 3D reconstruction and analysis.," Tech. Rep. 3595, INRIA, Sophia Antipolis, France, 1998.

[5] S. Sclaroff and A. Pentland, "Modal matching for correspondence and recognition.," *IEEE Transactions on Pattern Analysis and Machine Intelligence*, vol. 17, no. 6, pp. 545–561, June 1995.

[6] C. Nastar and N. Ayache, "Frequency-based nonrigid motion analysis: Application to four dimensional medical images.," *IEEE Transactions on Pattern Analysis and Machine Intelligence*, vol. 18, no. 11, pp. 1069–1079, 1996.

[7] C. Nikou, G. Bueno, F. Heitz, and J. P. Armspach, "A joint physics-based statistical deformable model for multimodal brain image analysis.," *IEEE Transactions on Medical Imaging*, vol. 20, no. 10, pp. 1026–1037, 2001.

[8] K. J. Bathe, *Finite Element Procedure*, Prentice Hall, Englewood Cliffs, New Jersey, 1996.

[9] G. Borgefors, "On digital distance transforms in three dimensions.," *Computer Vision and Image Understanding*, vol. 64, no. 3, pp. 368–376, 1996.

[10] A. Pentland and S. Sclaroff, "Closed-form solutions for physically-based shape modeling and recognition.," *IEEE Transactions on Pattern Analysis and Machine Intelligence*, vol. 13, no. 7, pp. 730–742, 1991.

[11] M. J. Black and A. Rangarajan, "On the unification of line processes, outlier rejection, and robust statistics with applications in early vision.," *International Journal of Computer Vision*, vol. 19, no. 1, pp. 57–91, 1996.

[12] S. Umeyama, "Least-squares estimation of transformation parameters between two point patterns.," *IEEE Transactions on Pattern Analysis and Machine Intelligence*, vol. 13, no. 4, pp. 376–380, April 1991.